Grinrey Conference Proceedings
ICMESR 2026, India, 04-05 May 2026
Volume 01 (2026) 001101
https://doi.org/10.55084/gcp/001101

CFD Analysis of Sequential Dual-Layer PCM Thermal Management for a Cylindrical Li-Ion Battery Using RT-35 and RT-42

Sarag Motghare[1,*] and Mahesh Kulkarni[1]

[1]Department of Mechanical Engineering, MIT World Peace University, Pune, India

Email: saragmotghare3@gmail.com ([*]Corresponding Author)

Received : 13 May 2026; Accepted : 16 Jul 2026; Published : 08 Aug 2026.

Abstract. Lithium-ion batteries are widely used in electric vehicles; however, their performance and safety are extremely sensitive to temperature increases during operation. Excessive heating can lead to thermal instability and thermal runaway, making effective thermal management critical. In this study, a transient Computational Fluid Dynamics (CFD) simulation of a dual-layer phase change material (PCM) cooling system for a cylindrical lithium-ion battery was performed using ANSYS Fluent 2024 R1. The model used the solidification and melting technique. RT-42 was employed as the inner PCM layer while RT-35 formed the outer layer in a concentric design. The battery core generated 726,000 W/m³ of heat during a continuous discharge of 12 W. Simulations were run for 1800 seconds. The creative element of this work is the sequential arrangement of dual layer PCMs with distinct melting ranges to achieve staged thermal regulation. The new aspect of this study is the unique dual-layer PCM arrangement, in which RT-42 is placed directly around the battery surface and RT-35 forms the outer annular layer. This arrangement allows sequential heat regulation during battery utilization. The temperature-time profile revealed two unique inflection points, representing the melting of RT-42 and RT-35, respectively. CFD-Post contour plots at t = 1800 s showed an active mushy zone near the battery-RT-42 interface, confirming latent heat absorption during phase change. A temperature drop of about 30 K was obtained between the battery core (435 K) and the outer RT-35 wall (405 K). This research demonstrated the effectiveness of the multi-stage passive thermal resistance concept for cylindrical lithium-ion cells under continuous discharge conditions.

Keywords**:** *ANSYS CFD; dual-layer PCM; lithium-ion battery; phase change material; thermal management*

1. INTRODUCTION

The worldwide energy crisis and environmental concerns have pushed the development of new energy electric vehicles (NEVs), which offer energy-saving and eco-friendly benefits[1]. Nowadays, Lithium-ion batteries are the top choice for NEVs because of their high energy density, extended cycle life, low self-discharge rate and quick charge/discharge capabilities[2]. However, their effectiveness and safety are strongly dependent on operating temperature. Statistics show an increase in fires caused by electric vehicles, leading to the thermal runaway issue of batteries[3]. The Battery Thermal Management System (BTMS) maintains the battery's temperature within the safe range (293.15 K - 318.15 K), with a maximum temperature difference of 5 K between the battery and the battery pack [4], [5]. As a result, the BTMS has developed with cooling methods [6].

 ISBN: 978-81-996627-3-5

Currently, cooling is classified into four categories: air cooling, liquid cooling, heat pipe cooling, and phase change material cooling[7]. Air cooling was initially promoted because of its simplest design and inexpensive cost. However, because of its poor heat capacity and weak thermal conductivity, it is not suitable for high-temperature settings or high discharge rate applications[8]. Alternatively, liquid cooling is the better option due to the high heat exchange. Because of the stringent sealing requirements and higher risk of short circuit from deterioration of the insulating materials, direct liquid cooling is not widely used in industry [9]. However, companies such as BYD and Tesla use indirect liquid cooling, which finds a balance between safety and cooling efficiency[2].A heat pipe is a highly thermally conductive element that moves heat by evaporating and condensing a working fluid inside a vacuum tube. Heat pipes have several benefits such as high thermal conductivity, isothermal effect, flexibility, reversibility, thermal stability and environmentally adaptable. They can however, create a temperature variation which demands additional cooling methods[10], [11]. In response to these limitations, passive, no energy consumption thermal management technology based on PCM has received a significant amount of interest, benefiting from the capability of absorbing a considerable amount of latent heat during the solid-to-liquid phase change to smooth out transient thermal spikes[12].

Srivastava conducted a parametric study in 2022 by combining experimental and numerical testing on a single 18650 cylindrical cell using RT-42 and Eicosane as PCMs, reporting peak surface temperatures of 316 K and 313 K respectively, at a discharge rate of 3C, highlighting the importance of PCM selection and melting point matching, as well as discharge conditions, for thermal buffering. However, they found that the effectiveness of the PCM decreased with the increase of ambient temperature, and the study was mainly conducted on single-layer PCM cooling[13]. In 2026, Zheng studied hybrid systems by combining PCMs with active cooling, using 21700 cylindrical cells with liquid cooling and dual layer vapor chambers. This experiment resulted in a maximum temperature of 309.53 K and a temperature difference of 4.56 K at a discharge rate of 4C, but with a high level of system complexity. Zhang et al. (2026) proposed a multi-stage thermal management system for lithium-ion batteries with multiple configurations of PCM layers.

The results demonstrated that the tiered PCM scheme could effectively enhance the heat dissipation and temperature uniformity, and significantly retard the propagation of thermal runaway. However, the study revealed the restriction of the PCM's low thermal conductivity, which hinders heat transfer efficiency without further thermal augmentation methods[7]. Despite these developments, few studies have looked into concentric dual-layer PCM topologies for cylindrical Li-ion batteries. In particular, no previous numerical work has investigated a contradictory PCM arrangement in which the higher-melting-point PCM (RT-42) is placed directly around the battery surface, while the lower-melting-point PCM (RT-35) forms the outside layer to achieve progressive temperature control.

While single-layer PCM based battery thermal management has received heavy attention recently, use of a dual-layer PCM system with sequential activating phases remains a major gap in the recent literature. Most prior research employed a single PCM with a set melting point, which either activates too early or too late (failing to respond to rapid thermal transients). The present study suggests a dual-layer arrangement incorporating RT-42 and RT-35, which are chosen to activate sequentially based on their different melting points, allowing for a two-stage thermal buffering response that adjusts to the battery's heat generation profile during the discharge cycle. The proposed configuration's key uniqueness is its sequential activation technique, as opposed to simultaneous or single-phase melting. RT-42 is used as the inner layer since it has the higher melting point (42°C), thus being exposed to the greatest amount of heat near the battery surface, where the heating process takes place most rapidly. This allows the inner layer to remain active through the peak heat-generation period without melting prematurely. RT-35 with the

lower melting point (35°C) is the outer layer that melts due to the lower intensity of the heating process caused by the protective function of the inner layer. In such a way, the two-stage melting process occurs when the first layer absorbs the heat produced initially and the second layer absorbs the residual part of heat. Conversely, if RT-35 were placed as the inner layer, it would melt prematurely. To close this gap, this research presents a CFD-based investigation of a dual-layer PCM thermal management system for cylindrical lithium-ion batteries, which employs RT-42 and RT-35 PCMs in a concentric dual-layer arrangement. The present study employs transient CFD simulations using ANSYS Fluent 2024 R1 to investigate the thermal behaviour of a novel dual-layer PCM configuration, consisting of an inner RT-42 annulus and an outer RT-35 annulus applied to a cylindrical lithium-ion cell under continuous 12 W discharge where for results the maximum core temperature were recorded. To represent the transient phase-change dynamics of both PCM layers, the Solidification and Melting model approach was used. CFD was chosen as this research methodology because it allows for spatial and temporal precision of temperature gradients and mushy zone evolution using only experimental instrumentation, without the cost and reproducibility limits of physical prototypes. The rest of the paper is organized as follows: Section 2 describes the computational geometry, material properties, governing equations, and solver configuration; Section 3 and 4 presents the CFD results and discussion and Section 5 summarizes the key conclusions of the paper.

2. METHODOLOGY

2.1 Geometry and Computational Domain

The simulation domain is built around a standardised cylindrical cell with a nominal outer diameter of 18 mm and a total length of 65 mm. The battery core is modelled as a solid, homogenous cylinder with a radius of 9 mm. The battery is encased in two concentric PCM annuli: RT-42 occupies the inner annular region, while RT-35 occupies the outer annular region. The geometry was created in ANSYS Space Claim 2024 R1 as three different solid bodies, as illustrated in the Fig.1. The zone dimensions are summarized in Table1.

Table 1. Computational domain zone geometry (All dimensions are in mm)

Zone	Inner Radius	Outer Radius	Axial Length	Role
Battery Core	0	9	65	Heat source (solid)
RT-42 (Inner PCM)	9	14	65	Primary thermal barrier
RT-35 (Outer PCM)	14	22	65	Secondary thermal barrier

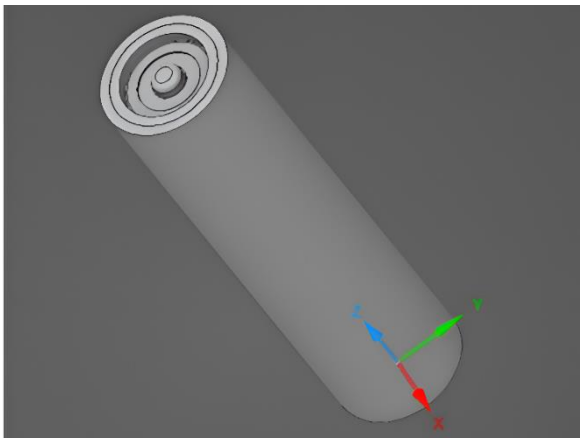

Fig. 1. Lithium-ion battery with dual-layer PCM

2.2 Material Properties

The material characteristics employed in our simulation setup are listed below in the Table 2 [14][15][16].

Table 2. Thermophysical properties assigned to each computational zone [3] [7][17][18]

Property	Battery Core	RT-42 (Inner)	RT-35 (Outer)
Density, ρ (kg/m³)	2500	880	860
Specific Heat, C_p (J/kg·K)	1100	2000	2000
Thermal Conductivity, k (W/m·K)	1.0	0.2	0.2
Solidus Temperature (K / °C)	—	311 / 38	305 / 32
Liquidus Temperature (K / °C)	—	318 / 45	311 / 38
Latent Heat of Fusion, L (J/kg)	—	165,000	157,000
Heat Generation, q‴ (W/m³)	726,000	—	—

2.3 Governing Equations

2.3.1 Energy Governing Equation

The transient heat transfer inside the battery and PCM domains is governed by the energy conservation equation[17]:

$$\rho C_p \frac{\partial T}{\partial t} = \nabla \cdot (k \nabla T) + q''' \quad (1)$$

Where, ρ= density (kg/m³), C_p= specific heat capacity (J/kg·K), T= temperature (K), k= thermal conductivity (W/m·K), and q'''= volumetric heat generation rate (W/m³).

2.3.2 Enthalpy Formulation for Pcm Melting

The total enthalpy of the PCM is expressed as[17][18]:

$$H = h_{ref} + \int_{T_{ref}}^{T} C_p \, dT + \beta L \quad (2)$$

Where, H is total enthalpy, h_{ref} is reference enthalpy, β is liquid fraction, and L is latent heat of fusion.

2.4 Mesh independence and Grid quality

In order to validate the accuracy of numerical results, a mesh independence and grid quality analysis was performed on three different mesh resolutions: coarse, medium and fine. They have a cell size equal to 2 mm, 1.5 mm, and 1 mm, respectively (Table 3). These meshes had the total number of cells of 662,169, 906,536 and 1,200,785 respectively. Additionally, the average orthogonal quality value is 0.807, 0.789 and 0.792 respectively, which is an acceptable value for conducting accurate solidification/melting simulation. In order to determine mesh independence, mass-weighted average temperature of the battery was analysed across these three different mesh resolutions (Table 4). Temperature difference between the coarse and medium mesh was just 0.0029% (from 411.4843 K to 411.4961 K), and between medium and fine mesh another 0.0009% (from 411.4961 K to 411.4924 K), showing a clear decreasing tendency with respect to the growing mesh resolution. Thus, as this small difference is acceptable in terms of numerical accuracy, solution was defined as mesh independent, and medium mesh (906,536 cells) was chosen for all further simulations.

Table 3. Grid Quality

Mesh	Element Size	Nodes	Elements	Avg. Orthogonal Quality
Coarse	2 mm	292,783	662,169	0.80705
Medium	1.5 mm	362,589	906,536	0.78933
Fine	1 mm	417,073	1,200,785	0.79245

Table 4. Mesh Independence

Mesh	Elements	Mass-Weighted Avg Temp (K)	% Change
Coarse	662,169	411.4843	-
Medium	906,536	411.4961	0.003
Fine	1,200,785	411.4924	0.0009

2.5 Solver Setup and Boundary Condition

The simulation was performed in ANSYS Fluent 2024 R1 as a transient, pressure-based solver using the laminar viscous model. Gravity was set to −9.81 m/s² in the axial (Z) direction, and the solidification and melting model was activated to allow for natural convection modelling in the liquid PCM phase. A time step of 2 seconds was used over 900-time steps, resulting in a total simulation period of 1800 seconds. A maximum of 20 inner iterations per time step was set. The outside surface of the RT-35 annulus was assigned a convective boundary condition with h = 10 W/m²·K and T∞ = 300 K. This represents conservative natural convection in calm air. All computing zones were initially set to a consistent temperature of 300 K. To imitate natural convection, a conservative externally convective heat transfer coefficient of h = 10 W/m²·K was used. The thermal stabilizing contribution of the PCM layers was purposely isolated without the need for artificial cooling. Throughout the 1800-second simulation, a steady volumetric heat generation rate corresponding to a continuous 12 W discharge was applied. The study used pure paraffin-based PCMs (RT35 and RT42) with a thermal conductivity of 0.2 W/m·K, which matches the standard unenhanced paraffin values described in the literature. The solver settings are summarized in Table 5

Table 5. CFD solver configuration and boundary conditions

Parameter	Value / Configuration
Solver type	Pressure-based, transient
Viscous model	Laminar
Energy equation	Enabled
Solidification & melting model	Enabled; A mush = 1×10^5
Gravity	−9.81 m/s² (Z-direction)
Time step size	2 s
Total simulation duration	1800 s (30 min)
Number of time steps	900
Max iterations per time step	20
Outer boundary (convection)	h = 10 W/m²·K, T∞ = 300 K
Initial temperature (all zones)	300 K (27°C)

3. RESULTS

3.1 Global Thermal Distribution Analysis

Fig. 2-4 show the layer-by-layer global temperature contours of the battery-PCM assembly at t = 1800 s, with a similar colour scale spanning from 299.1 K to 434.9 K allowing for direct cross-comparison across all three domains. In Fig. 2, the battery core and the inner RT-42 surface exhibit a prominent orange-yellow thermal field within the temperature range of 367- 421 K, with the highest temperature concentrated at the battery surface due to the applied volumetric heat source. The concentric ring pattern observed at the top end-cap indicates radially symmetric heat conduction, thereby confirming the geometric symmetry and validating the numerical model. Moving outward to the RT-42/RT-35 interface (Fig. 3), the dominant colour shifts to a mixed orange-yellow field with emerging yellow banding, corresponding to an interface temperature of 355-410 K, a reduction of 11-24 K relative to the battery core due to latent heat absorption within the RT-42 mushy zone, where the solid-liquid phase transition intercepts outward heat flux. The most distant RT-35 surface (Fig. 4) has the highest thermal contrast, with a constant yellow-green field representing the total radial temperature in the range of 340-405 K. The reduction is about 30 K from the battery core to the outer PCM layer. The physical uniformity of this outer thermal field, without any localised hotspots, proves that RT-35 acts as an extra thermal buffer, which minimizes and evenly distributes the residual heat flux passing through the RT-42 annulus. The systematic colour-band shift across the three contours of orange-yellow (Fig. 2), orange-yellow with emerging yellow (Fig. 3), and uniform yellow-green (Fig. 4) provides direct visual and quantitative evidence of the study's central design contribution: the stepped, layer-by-layer radial thermal resistance mechanism.

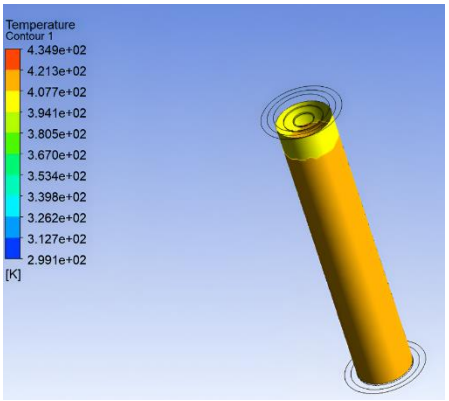

Fig. 2. Battery/RT-42 interface temperature distribution (299-435 K)

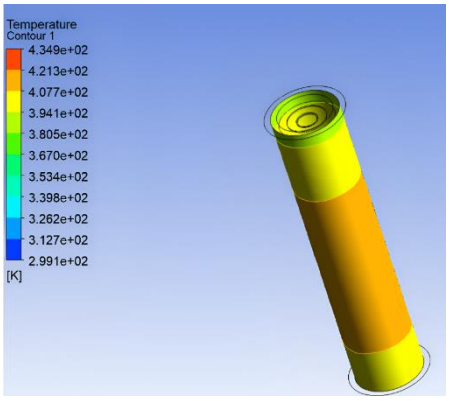

Fig. 3. RT-42/RT-35 interface temperature distribution (299-435 K)

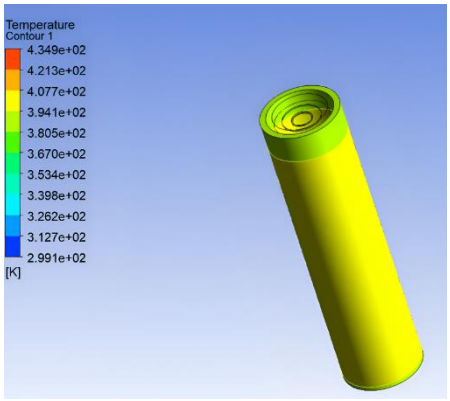

Fig. 4. RT-35 outer surface temperature distribution (299-435 K)

3.2 Cross Sectional Analysis

Cross-sectional plane cuts at the battery centre (z = 32.5 mm) were visualized using CFD-Post, with two different scales: a local range (Fig. 5) to maximize contrast outside the high-temperature near-cell region. Fig. 5 uses a local scale to emphasize contrast within the high-temperature near-cell region, while Fig. 6 uses a global scale to show the full radial gradient. To explain the whole radial gradient, including the outer annulus of RT-35, a global scale is used (Fig. 6). The photos show that the temperature is highest at the core of the battery (red, ~430-434 K) and as we move radially outwards through the RT-42 annulus (orange, ~410-430), it slowly decreases. Further into the outer annulus of the RT-35 (yellow-green, ~380-

410 K), the temperature drops to 380K. These represent a steady decrease in temperature across the layered domains. The dual-PCM layer is seen absorbing heat progressively along the outward temperature gradient. The heat flux is divided by the layers, each annulus of PCM intercepting a part of the heat flux before it reaches the next annulus outer surface.

The inner edge of the annulus of the RT-42 is not circular but rather has an irregular shape as shown in both figures. Under optimum conductive conditions, the solid-liquid contact is a full concentric contact ring. The irregularity seen here indicates that natural convection is present in the molten RT-42. Hot liquid in the melt rises because of buoyancy, causing heat transfer to be non-uniform annulus. This shows that the simulation is a true representation of real-life phase change behaviour and not a simplified idealised melt front.

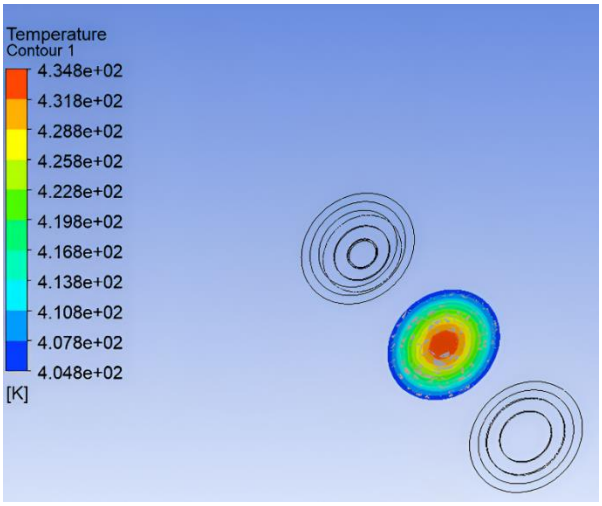

Fig. 5. Mid-section local temperature distribution (404-434 K)

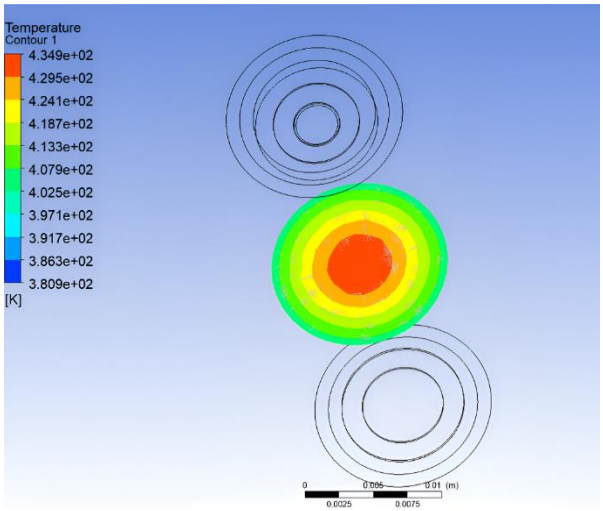

Fig. 6. Mid-section global temperature distribution (380-434 K)

3.3 Local Thermal Distribution

In Fig. 7-9, the local contour plots are displayed for each of the domains and are scaled to their own layer's temperature range, which gives a more accurate and thorough impression of the thermal status for each PCM zone at t = 1800 seconds. Temperatures at the Battery/RT-42 interface (Fig. 7) range from 397 to 419 K, peaking at the battery surface. It is the principal source of heat as shown by the presence of this surface. The combination of red, orange and green regions on the RT-42 surface signifies that the surface is still going through phase change. Latent heat absorption and local temperature regulation continue outward to the RT-42/RT-35 contact (Fig. 8), where the temperature range decreases to 385-410 K, indicating that RT-42 has absorbed the most of the heat before reaching the outer layer. Finally, the RT-35 outer wall (Fig. 9) shows a further reduced temperature range (380–405 K), indicating that it remains thermally active and helps in regulating battery temperature. Overall, these results demonstrate that both PCM layers are thermally active and functioning, with each layer independently collecting heat. This layer-by-layer heat collection contributes to the overall uniformity of the radial thermal gradient from the core to the surface.

3.4 Transient Temperature Evolution

Fig.10 depicts the battery-PCM system's transient temperature response throughout a simulated duration of 1800 seconds. The transient reaction can be divided into three physically distinct phases, each defined by a noticeable shift in the rate of temperature rise:

Phase I - Sensible Heating (t = 0 to ~400 s): The system temperature rapidly increases from the uniform initial condition of 300 K. During this phase, all three zones absorb the majority of the energy input from the battery core as perceptible heat. The rate of temperature rise reaches its maximum, which is determined by the battery-PCM assembly's aggregate sensible heat capacity.

Phase II - RT-42 Primary Activation (~400 s to ~900 s): The local temperature at the battery-RT-42 interface rises into the RT-42 melting range. The rate of temperature rise begins to decrease as RT-42 activates, resulting in a significant drop in the rate of temperature rise. The average temperature rises throughout this phase, although at a far slower rate than in Phase I, as the inner PCM gradually absorbs the latent energy load.

Phase III - RT-35 Secondary Activation (~900 s to 1800 s): As thermal energy propagates through the RT-42 layer and reaches the RT-42/RT-35 contact, the temperature at that boundary climbs through the RT-35 melting range, causing the second PCM layer (RT-35) to activate. As both PCM layers absorb latent heat simultaneously during this phase, the system temperature rise rate slows further, nearing a near-asymptotic plateau around 406-408 K near t = 1800s.The gradual slowdown of temperature rise throughout these three phases provides direct numerical evidence of the multi-stage passive thermal resistance mechanism that this setup was intended to provide**.**

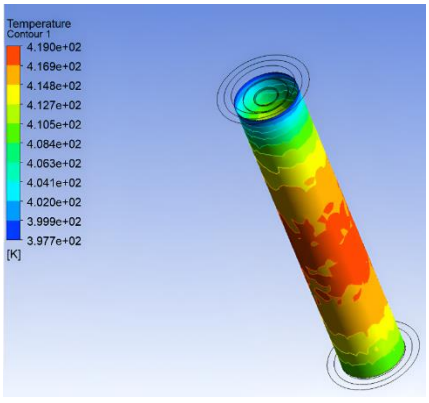

Fig. 7. Battery/RT-42 interface temperature distribution (397-419 K)

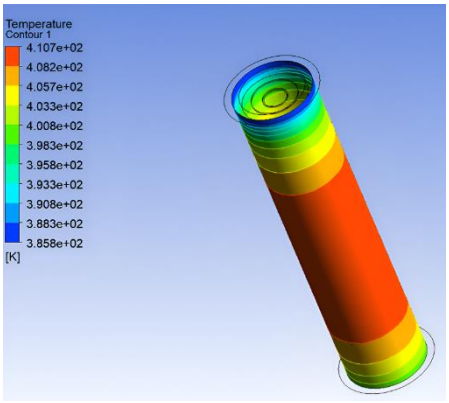

Fig. 8. RT-42/RT-35 interface temperature distribution (385-410 K)

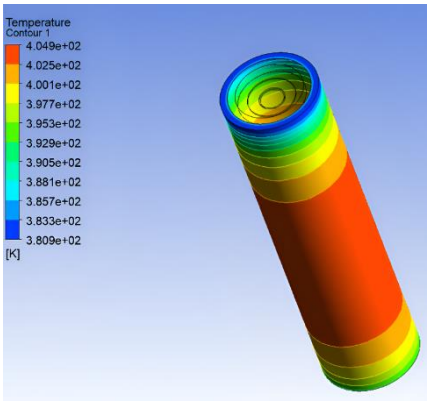

Fig. 9. RT-35 outer surface temperature distribution (380-405 K)

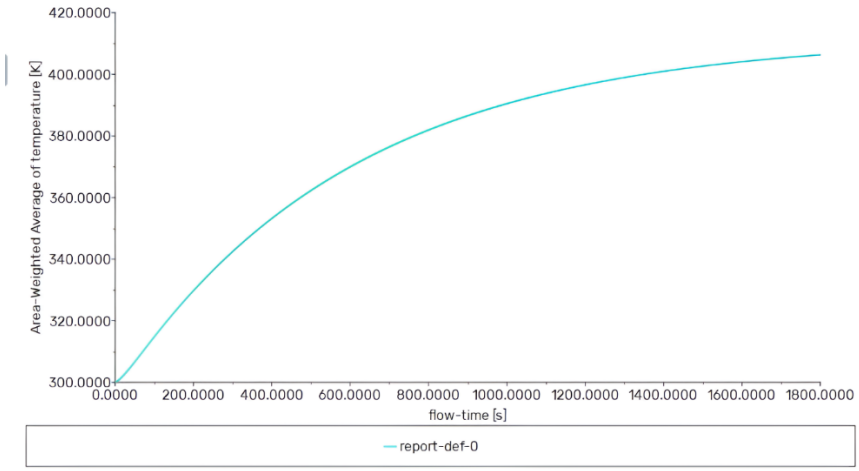

Fig. 10. Average Battery Temperature vs Time Graph

3.5 Solver Convergence and Numerical Stability

The simulation ran for 900-time steps (2 seconds each), resulting in a total simulation time of 1800 seconds as shown in Fig.11 Convergence at each time step was assessed using scaled residuals for the energy and continuity equations. The energy residual converged smoothly from 1×10^{-5} to less than 1×10^{-8} by the end of the simulation, suggesting good overall convergence. A significant surge in residuals was seen around iteration 1000, coinciding with the peak phase-change activity in the RT-42 mushy zone, following which residuals fell smoothly as both PCM layers stabilized post-melt.

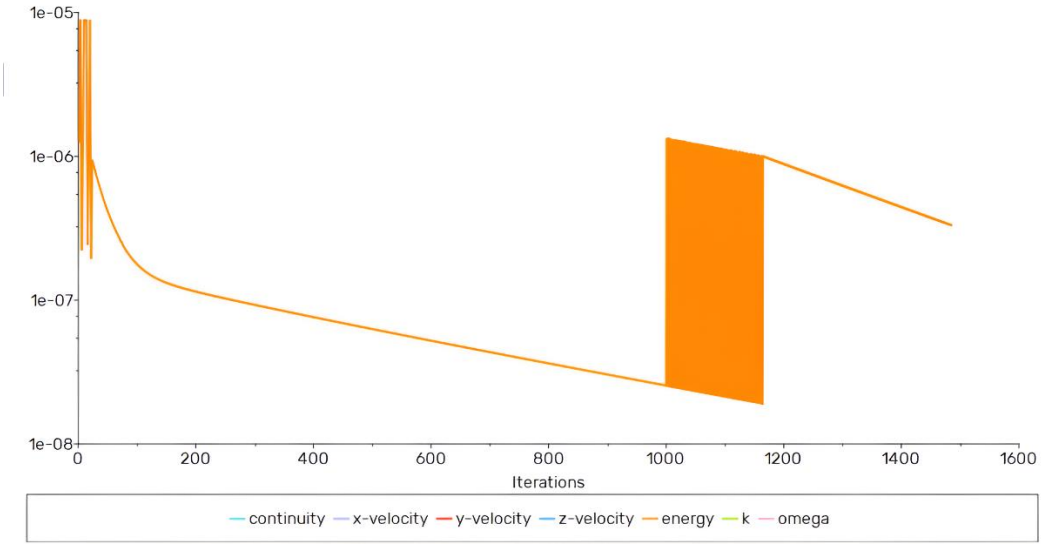

Fig. 11. Residual convergence history

3.6 Model Validation

As no directly equivalent dual-layer configuration exists in the open literature, quantitative benchmarking against prior studies is not meaningful. Instead, the present model is validated through internal physical consistency: the formation of a mushy zone at the melting front (Fig. 2, 7), the monotonic radial temperature decay consistent with Fourier's law (Fig. 5, 6), and most notably the appearance of temperature-time inflection points precisely at the independently specified melting ranges of RT-42 (311–318 K) and RT-35 (305–311 K) in Table 6. This agreement between the input material properties and the emergent thermal response confirms the enthalpy-based solidification/melting formulation is functioning correctly, independent of any external dataset

3.7 Summary of Key Results At T=1800s

Table 6. Temperature results at t = 1800 s

Zone / Location	Temp (K)	Temp (°C)	PCM Status
Battery core (max)	434	161	Heat source
Battery/RT-42 interface	419	146	RT-42 mushy zone
RT-42/RT-35 interface	410	137	Heat stepped down
Outer RT-35 wall	405	132	RT-35 active
Bottom face (min)	299	26	Near ambient
Total temperature drop (core to outer wall)	~30	~30	PCM effective

4. DISCUSSION

There is a significant rise in the battery internal temperature because of the high rate of heat production in per unit volume (726,000 W/m^3). In addition to that, there is low thermal conductivity in the phase change material layer which results in a limitation of heat transfer to the outside surface. During practical use of EVs, such high core temperatures without proper control can cause faster reduction in the capacity of the battery, increased internal resistance and in extreme cases, thermal runaway. The dual-layered PCM case study is thus directly relevant for practical applications as it decreases the maximum core temperature. This is because paraffin-based PCMs have a thermal conductivity of 0.2 $W/m \cdot K$, which is nearly 200 times lower than aluminium. This limits forward heat diffusion through the bulk PCM, despite effective latent heat absorption at the solid-liquid interface, causing heat to accumulate on the battery surface. To address this, feasible options use graphite filler or metal foam to increase effective conductivity to around 1.0-1.5 $W/m \cdot K$. The convective heat transfer coefficient of $h = 10\ W/m^2 \cdot K$, which represents the minimal threshold for natural convection in still air, was intentionally used to isolate the single thermal contribution of the PCM. However, genuine EV battery packs use additional forced air or liquid cooling to considerably reduce outside surface temperatures. Furthermore, the continuous 12 W heat generation imposed over 1800 seconds with no rest interval is a worst-case thermal stress state rather than normal discharge behaviour.

In fact, discharge-rest cycles enable the PCM to re-solidify and regain its latent heat capacity between successive heat events, considerably enhancing thermal management effectiveness. Despite these conservative conditions, the key finding is validated: the dual-layer PCM system generates a clear, measurable 30 K temperature gradient from the battery surface to the outer wall, with both PCM layers confirmed to be active (RT-42 mushy zone at the battery interface and RT-35 active in the outer annulus). The radial temperature differential generated by the dual-PCM enclosure under these worst-case conditions is thus the major performance metric of this study, rather than the absolute temperature. The 30 K temperature gradient observed between the battery core (434 K) and the exterior RT-35 wall (405 K) quantitatively verifies the multi-stage latent heat buffering idea. Furthermore, the proven sequential activation of both PCM layers (RT-42 mushy zone at the battery interface, RT-35 active in the outside annulus) plainly illustrates the counter-intuitive inner-outer PCM coupling placing the higher-melting-point material in touch with the battery surface. In addition, analysis of thermal performance indicators in comparison to recent research clearly indicates that there is an advantage of sequential dual-layer system over the existing single-layer systems. For example, even though Srivastava (2022) [13] succeeded in proving that the single-layer RT-42 and Eicosane had good thermal buffering capabilities under 3C discharge conditions, the single-layer systems were susceptible to early melting as a consequence of long-term thermal transients. As soon as one PCM layer fully melts, the process of sensible heating starts, resulting in sudden temperature increase. On the other hand, even though Zhang et al. (2026) [7] confirmed the effectiveness of multiple stage PCM systems in delaying thermal runaway progression, they emphasized that the unmodified PCM layers experienced the problem of poor heat dissipation caused by low thermal conductivity. With high-melting-point RT-42 directly connected to the cell surface and combined with an outer RT-35 annular structure, our design provides for a staged radial decrease in temperature of 30 K. The synergistic combination of these two materials effectively prevents the outer boundary from premature melting, which enhances thermal buffering time compared to single-phase systems.

5. CONCLUSION

The ANSYS Fluent 2024 R1 was used to perform a transient CFD simulation of a dual-layer PCM thermal management system for a lithium-ion battery cell. The multi-stage PCM configuration created a sequential thermal barrier mechanism in which the inner RT-42 layer primarily absorbed latent heat during Phase II of discharge, resulting in a reduced rate of temperature rise, while the outer RT-35 layer served as a secondary thermal barrier during Phase III by absorbing the residual heat flux passing through the RT-42 annulus. At t = 1800 s, a persistent radial temperature differential of approximately 30 K was observed between the battery core and the outside RT-35 wall, confirming the multi-stage thermal resistance. Additionally, the non-uniform mushy zone patterns at the battery-RT-42 interface revealed active latent heat absorption and realistic phase change behaviour. The energy residuals reached 1×10^{-8}, indicating sustained convergence of the solver during the simulation. The transient residual rise near t = 400 s was due to peak mushy zone activity rather than numerical instability. The designed two-layer PCM system provides an efficient, maintenance-free thermal management method that is effective in compact EV battery pack systems especially in cases where active cooling (through pumps and fans) increases weight, cost, and energy consumption. The system works sequentially and hence can be used in driving cycles that involve sudden high load discharges (such as acceleration or regenerative braking). Nevertheless, the ability of the system to perform depends on the amount of latent heat capacity provided by the PCM layers, and hence in cases where high loads persist (such as fast charging or continuous high speed driving), there comes a point when the PCM melts completely and hence cannot act as a buffer any more, resulting in temperature increase based on conduction only. Another limitation of this system is that PCM cycling leads to loss of performance, but this was not considered in this study. The results show that the dual-layer PCM architecture is effective in achieving sequential latent heat absorption, greater thermal resistance, and consistent phase-change behaviour. This highlights its potential for improved thermal management of lithium-ion batteries.

ACKNOWLEDGEMENT

The authors would like to thank the Department of Mechanical Engineering, MIT-WPU, Pune for providing the necessary computational resources and support for this research.

REFERENCES

[1] L. Zhang, H. Zhao, and C. Liu, “Thermal management for transient integrated battery and power electronics systems using phase change materials,” *International Journal of Thermal Sciences*, vol. 209, Mar. 2025. [CrossRef] [Publisher]

[2] D. Zheng, X. Chen, X. Han, and N. Chu, “Performance study and optimization of a hybrid liquid cooling integrated with vapor chamber and phase change material for cylindrical lithium-ion battery,” *Applied Thermal Engineering*, vol. 290, Apr. 2026. [CrossRef] [Publisher]

[3] C. Zhao, W. Hu, D. Meng, W. Mi, X. Wang, and J. Wang, “Full-scale experimental study of the characteristics of electric vehicle fires process and response measures,” *Case Studies in Thermal Engineering*, vol. 53, Jan. 2024. [CrossRef] [Publisher]

[4] D. R. Pendergast, E. P. Demauro, M. Fletcher, E. Stimson, and J. C. Mollendorf, “A rechargeable lithium-ion battery module for underwater use,” *Journal of Power Sources*, vol. 196, no. 2, pp. 793–800, Jan. 2011. [CrossRef] [Publisher]

[5] Z. Wang, R. Bao, N. Zhang, S. Hong, Q. Gao, and H. Yang, “Performance study and optimization of battery thermal management system for integrated cooling/heating of cylindrical lithium-ion battery modules,” *Journal of Energy Storage*, vol. 147, Feb. 2026. [CrossRef] [Publisher]

[6] A. Khan *et al.*, “A state-of-the-art review on heating and cooling of lithium-ion batteries for electric vehicles,” Jan. 2024. [CrossRef] [Publisher]

[7] Y. Zhang *et al.*, “Design and performance analysis of a multi-stage phase change material-based thermal management system for lithium-ion batteries,” *Journal of Power Sources*, vol. 670, Apr. 2026. [CrossRef] [Publisher]

[8] M. Murugan *et al.*, "Thermal management system of lithium-ion battery packs for electric vehicles: An insight based on bibliometric study," *Journal Energy Storage*, vol. 52, August 2022. [CrossRef] [Publisher]

[9] L. Martellucci, R. Capata, and M. De Marco, "Comparative Review of Cooling Systems for Lithium-Ion Battery Modules with 21700 Cylindrical Cells," March. 2026. [CrossRef] [Publisher]

[10] Y. Zhao, B. Zou, J. Ding, and Y. Ding, "Experimental and numerical investigation of a hybrid battery thermal management system based on copper foam-paraffin composite phase change material and liquid cooling," *Applied Thermal Engineering.*, vol. 218, Jan. 2023. [CrossRef] [Publisher]

[11] C. Hu, H. Li, Y. Wang, X. Hu, and D. Tang, "Experimental and numerical investigations of lithium-ion battery thermal management using flat heat pipe and phase change material," *Journal of Energy Storage*, vol. 55, Nov. 2022. [CrossRef] [Publisher]

[12] A. Calborean, L. Máthé, and O. Bruj, "Phase Change Materials for Thermal Management in Lithium-Ion Battery Packs: A Review," Dec. 2025. [CrossRef] [Publisher]

[13] G. Srivastava, R. Nandan, and M. K. Das, "Thermal runaway management of Li ion battery using PCM: A parametric study," *Energy Conversion and Management: X*, vol. 16, Dec. 2022. [CrossRef] [Publisher]

[14] P. Ping, Y. Zhang, D. Kong, and J. Du, "Investigation on battery thermal management system combining phase changed material and liquid cooling considering non-uniform heat generation of battery," *Journal of Energy Storage*, vol. 36, Apr. 2021. [CrossRef] [Publisher]

[15] Rubitherm Technologies GmbH, "RT42 Data Sheet," Berlin, Germany, Rev. 09.10.2020, Accessed on 20 February 2026. [Publisher]

[16] Rubitherm Technologies GmbH, "RT35 Data Sheet," Berlin, Germany, Rev. 18.04.2024, Accessed on 20 February 2026. [Publisher]

[17] F. Alimi *et al.*, "Artificial intelligence - computational fluid dynamics study close contact melting of phase change materials in a finned shell-tube energy storage," *Case Studies in Thermal Engineering*, vol. 75, p. 107015, Nov. 2025. [CrossRef] [Publisher]

[18] Y. Xu, J. Shi, X. Nie, X. Liu, and G. Liu, "Design and thermal performance analysis of a novel dual-layer cascade phase change battery thermal management system," *Journal of Energy Storage*, vol. 100 B, Oct. 2024. [CrossRef] [Publisher]